Chem

CellPress

Article

Organometallic lanthanide bismuth cluster single-molecule magnets

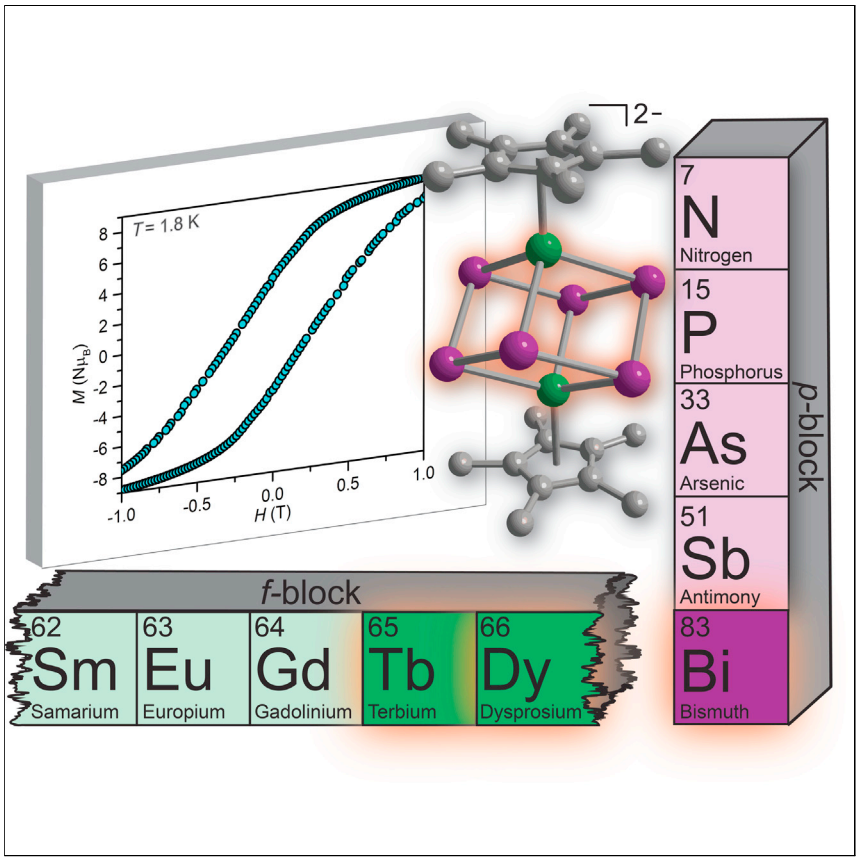

Synthesis of lanthanide bismuth cluster complexes were accomplished with a solution organometallic approach. The core is a heterometallocubane consisting of two highly anisotropic lanthanide ions bridged by an unprecedented Bi_6^{6-} Zintl ion, which promotes effective magnetic superexchange. This gives rise to open magnetic hysteresis loops, which is unprecedented for bismuth-containing molecules and, thus, introduces bismuth into the design handbook for single-molecule magnets.

Peng Zhang, Florian Benner, Nicholas F. Chilton, Selvan Demir

sdemir@chemistry.msu.edu

Highlights

Isolation of organometallic *f*-element bismuth cluster complexes

Heterometallocubane $[Ln_2Bi_6]$ featuring two lanthanides bridged through a Bi_6^{6-} unit

Single-molecule magnets containing bismuth donors

Magnetic hysteresis in superexchange-coupled lanthanide complexes

Zhang et al., Chem *8*, 717–730
March 10, 2022
https://doi.org/10.1016/j.chempr.2021.11.007

Chem

CellPress

Article

Organometallic lanthanide bismuth cluster single-molecule magnets

Peng Zhang,[1] Florian Benner,[1] Nicholas F. Chilton,[2] and Selvan Demir[1,3,*]

SUMMARY

Single-molecule magnets (SMMs) are molecules that can retain magnetic polarization in the absence of an external magnetic field and embody the ultimate size limit for spin-based information storage and processing. Multimetallic lanthanide complexes lacking magnetic exchange coupling enable fast relaxation pathways that attenuate the full potential of these species. Employment of diamagnetic heavy main group elements with diffuse orbitals may lead to unprecedented strong coupling. Herein, two bismuth-cluster-bridged lanthanide complexes, $[K(THF)_4]_2[Cp^*_2Ln_2Bi_6]$ (Cp^* = pentamethylcyclopentadienyl; 1-Ln, Ln = Tb, Dy), were synthesized via a solution organometallic approach. The neutral $[Ln_2Bi_6]$ heterometallocubane core features lanthanide centers that are bridged by a rare Bi_6^{6-} Zintl ion, which supports strong ferromagnetic interactions between lanthanides. This affords the rare observation of magnetic blocking and open hysteresis loops for superexchange-coupled SMMs comprising solely lanthanide ions. Both compounds constitute the first SMMs containing bismuth donors paving the way for promising synthetic targets for quantum computation.

INTRODUCTION

Molecular magnetism is a textbook example of synergetic effects arising from the interplay of chemistry and physics that composes a vibrant, multidisciplinary, and established research field.[1] The development of the field relies on the design and synthesis of new molecules, followed by thorough magnetic, spectroscopic, and theoretical investigations.[2] In particular, synthetic inorganic chemistry enables access to a wide range of organic, coordination, and organometallic compounds bearing signatures of interesting single-molecule magnet (SMM) behavior.[3] Lanthanides (Ln) are especially well suited for the design of SMMs due to their large magnetic anisotropy originating from near-unquenched orbital angular momentum and strong spin-orbit coupling.[4] Recently, the judicious optimization of crystal field resulted in magnetic bistability persisting up to liquid nitrogen temperature in a mononuclear Dy-based metallocene complex, representing the current performance record for a SMM.[5] A parallel strategy exploits the synthesis of multimetallic systems, where in addition to tailored crystal fields, the magnetic communication between highly anisotropic lanthanide centers is of utmost importance. However, multimetallic lanthanide complexes with requisite large spin ground states pose a synthetic challenge since the contracted 4*f*-orbitals of the metal centers only engender weak magnetic exchange.[6] Here, several viable strategies have resulted in significant breakthroughs in the design of high-performance SMMs via enhancing magnetic coupling to lanthanide ions, which includes, but is not limited to, the coupling through *nd* metal ions, radical ligands, and single-electron Ln–Ln bonds stabilized as endohedral metallofullerenes (EMFs).[7–12] Albeit synthetically

The bigger picture

Single-molecule magnets are molecules that act as nanoscopic analogs to classical magnets and have garnered substantial interest due to their potential applications in high-density information storage, magnetic refrigeration, spin-based electronics, and quantum computation. To realize such applications, memory loss needs to be prevented, which requires judicious design of coordination complexes. Herein, we developed a strategy to unprecedented organometallic SMMs comprising lanthanide and bismuth ions that exhibit magnetic memory. The core heterometallocubane includes bismuth and lanthanides and was hitherto unknown. Despite the contracted nature of the lanthanide 4*f*-orbitals, the bismuth cluster allows significant magnetic superexchange, thus defining a new platform for SMM design. This peerless class of compounds leads also to new prospects in physics and synthetic chemistry.

challenging, the implementation of radical-bridging ligands has proven to be a particularly successful approach, which is attributed to the diffuse radical spin orbitals that are able to penetrate the core electron density of the 4*f*-orbitals resulting in enhanced magnetic exchange coupling to lanthanide centers. The successful stabilization, isolation, and purification of lanthanide radical SMMs occurred with bridging radicals, which gave rise to open magnetic hysteresis loops comprising a giant coercive field of approximately 8 T for a SMM.[10,13,14] Although a desirable approach, the generation of radical-bridges necessitates redox-active ligands, which dramatically limits the number of target molecules and adds an additional layer of sensitivity and reactivity of the compounds due to the open-shell ligands employed. A promising route to SMMs that show magnetic memory at high temperatures is to enhance magnetic exchange between the lanthanide centers using diamagnetic heavy *p*-block donor atoms, since their diffuse valence orbitals may facilitate better penetration of the core electron density of the lanthanide ions and better energy matching, compared with the more commonly employed diamagnetic ligands with lighter C/N/O/Cl donor atoms.[15] This theory is supported by observations, such as the doubled magnetic exchange interaction in the sulfur-bridged dinuclear dysprosium SMM, $[(C_5H_4Me)_2Dy(\mu\text{-}SSiPh_3)]_2$, compared with the similar chloride-bridged complex, $[Cp_2Dy(thf)(\mu\text{-}Cl)]_2$, which consequently results in more efficient mitigation of quantum tunneling relaxation processes at low temperatures.[16]

The exploration of ligands containing heavier main group elements for the construction of SMMs is scarce.[15] Noteworthy is a series of Dy-based SMMs containing Dy^{III}–P, Dy^{III}–As, and Dy^{III}–Sb bonds, which demonstrated the critical role in moderating the magnitude of barriers to spin relaxation (U_{eff}) among the different pnictogen donors, showing decreasing coordination ability from P, As to Sb.[17–19] Similarly, the impact of covalent bonding on magnetic relaxation dynamics was also illustrated in Dy-based SMMs bearing Dy^{III}–Ge^{II} and Dy^{III}–Sn^{II} bonds, respectively, where the former features stronger Dy^{III}–Ge^{II} bonding in the equatorial position leading to a lower effective spin-reversal barrier and faster quantum tunneling of the magnetization.[20] Notably, magnetic blocking derived from coupled states has been observed in multinuclear systems, such as 3*d*-4*f* clusters,[7] radical-bridged lanthanide complexes,[13] and EMFs,[21] where each coupled system operates as a single magnetic unit for the reversal of magnetic moment akin to transition metal cluster complexes. In contrast, such magnetic blocking remains rare for purely lanthanide-based polynuclear SMMs containing diamagnetic bridges between lanthanide centers. In those systems, the observed slow magnetic relaxation is ascribed to the single-ion effect.[7,8,22] Thus, we pursued the design of cluster complexes consisting of late lanthanide ions and heavy main group element bridges. The latter will engender strong magnetic exchange coupling between lanthanide centers to potentially afford sufficient energy separation between exchange-coupled levels for blocking the reversal of magnetization.

Bismuth was long thought to be the heaviest non-radioactive element of the periodic table.[23] It possesses high principle quantum number valence orbitals (6*s*), and features effects arising from strong spin-orbit coupling. These characteristics create different effects on crystal field and magnetic exchange interactions with metal centers, when compared with the properties arising for its lighter group V homologs.[24] To the best of our knowledge, no SMM with a coordinating bismuth ion to one or more anisotropic metal centers have been reported. Moreover, complexes that contain both transition metal and bismuth ions are exceedingly rare, and magnetic studies on these are even scarcer. In a remarkable Mn^{II}–Bi^{III} heterobimetallic

[1]Department of Chemistry, Michigan State University, 578 South Shaw Lane, East Lansing, MI 48824, USA

[2]Department of Chemistry, the University of Manchester, Manchester M13 9PL, UK

[3]Lead contact

*Correspondence: sdemir@chemistry.msu.edu

https://doi.org/10.1016/j.chempr.2021.11.007

complex exhibiting the shortest known Mn–Bi distance, the transfer of spin-orbit coupling effects in diamagnetic Bi^{III} ion to the spin-bearing isotropic Mn^{II} ion was elucidated by examining the axial zero-field splitting parameter of the Mn^{II} center, which resembles the heavy atom effect observed in heavy halide species.[25] Bismuth is a poor coordinating donor ligand owing to unsupported hard-soft linkages and is thus challenging to employ for *f*-element chemistry.[26,27] Only one dinuclear complex containing Sm^{III} and Bi ions is known,[28] along with a handful of intermetalloid cluster complexes featuring Zintl ions.[29–32]

The unique electronic and physical properties associated with lanthanide and bismuth ions, respectively, sparked our interest to develop magnetic molecules containing both highly magnetically anisotropic lanthanides and bismuth ions. If the major synthetic challenges of their preparation can be overcome, Ln–Bi species will enrich 4*f* and main group chemistry, paving the way to discoveries of new structure types and magnetic phenomena. Here, we report the isolation of the first bismuth-cluster-bridged dilanthanide complexes, $[K(THF)_4]_2[Cp^*_2Ln_2Bi_6]$ (Cp^* = pentamethylcyclopentadienyl; **1-Ln**, Ln = Tb, Dy), where the two lanthanide centers are connected through an exceptional Bi_6^{6-} unit, forming a unique Ln_2Bi_6 heterometallocubane. Notably, neither a metallocubane core of formula M_2Bi_6, nor a Bi_6^{6-} moiety in any organometallic compound, have yet been reported. Significantly, ferromagnetic interactions between the two lanthanide centers mediated through the Bi_6^{6-} bridge led to the observation of open magnetic hysteresis at low temperatures in superexchange-coupled Ln-SMMs.

RESULTS AND DISCUSSION

Synthetic considerations

Among the few reported, primarily solid-state compounds that contain Ln–Bi fragments, intermetalloid clusters involving Zintl ions are most relevant to this study. These clusters exhibit stronger coordinating ability to metal centers via *p*-orbital bonding electrons than do single-site bismuthine ligands (BiR_3 or BiR_2^-).[29–32] The general synthetic route for intermetalloid clusters comprising heavy main group and *d*- or *f*-elements starts with an intermetallic Zintl complex, which is prepared via a solid-state reaction involving alkali metals and heavy main group elements.[33,34] The synthetic protocol then requires highly polar solvents, such as ethylenediamine, in order to dissolve the starting materials and products.

Drawbacks of these synthetic routes include low yields of the desired products and unavoidable byproducts, which precludes scalable syntheses of pure intermetalloid cluster compounds and, as a result, prevents studies of their chemical and physical properties.[35] Modification of Zintl ions or intermetalloid clusters through the coordination of organic or organometallic ligands shows great promise for improving the solubility, stability, reactivity, and purification of these products.[36] Therefore, the development of a facile solution synthetic route to cluster complexes, which readily allows product isolation and purification is highly desirable and demands judicious selection of suitable bismuth and lanthanide starting materials.

Decamethylsamarocene, containing highly reducing Sm^{II}, produced in solution the only known lanthanide bismuth molecule.[28] Its formation hints at redoxchemistry being generally crucial for the generation of lanthanide bismuth complexes. Importantly, due to their unfavorable reduction potentials, an analogous soluble divalent precursor reagent is not available for the highly anisotropic metals Tb and Dy, which are prevalent in molecular magnetism owing to their large magnetic anisotropy.[37] In addition, the construction of Bi–Bi bonded compounds containing single or multiple

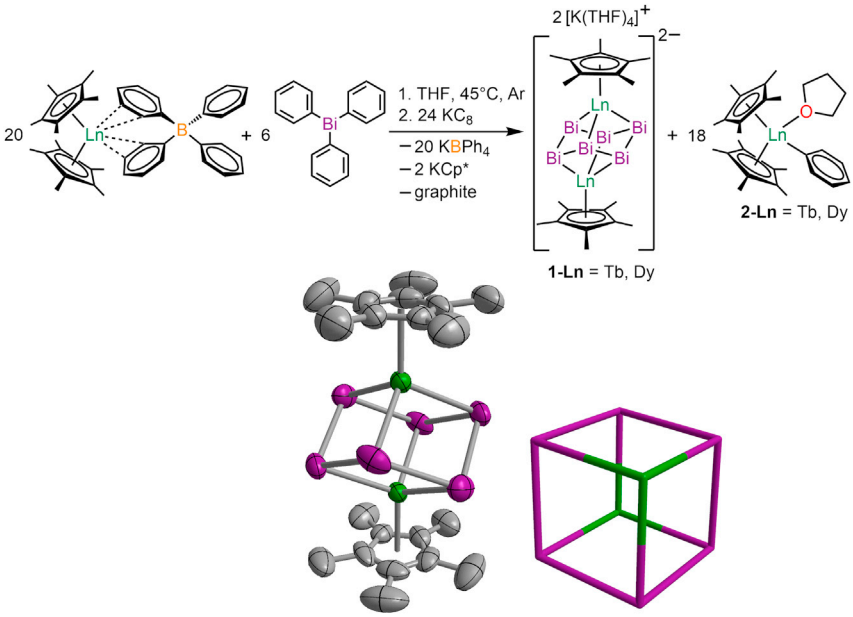

Figure 1. Synthesis and structure of the cluster complexes

(Top) Synthetic scheme for **1-Ln** (Ln = Tb, Dy). (Bottom, left) Thermal ellipsoid plot of the organometallic lanthanide bismuth cube dianion in a crystal of **1-Dy**, drawn at the 50% probability level. (Bottom, right) Neutral (Ln_2Bi_6) cube-shaped core enlarged. Green, purple, and gray spheres represent Ln, Bi, and C atoms, respectively. H atoms have been omitted for clarity. **1-Tb** is isostructural with **1-Dy**.

bonds via direct reductive coupling of organobismuth compounds (BiR_3, BiR_2X, $BiRX_2$, and $BiCl_3$) is possible in solution.[38]

The complexes $[K(THF)_4]_2[Cp^*_2Ln_2Bi_6]$, **1-Ln**, were synthesized by mixing $Cp^*_2Ln(BPh_4)$ (Ln = Tb, Dy)[39] and triphenylbismuth in THF and subsequent reduction with potassium graphite at 45°C (Figure 1; Tables S1 and S2). The addition of KC_8 generates highly reducing species that reduce Bi^{III} to Bi^{-I}, enabling the formation of the cluster complexes **1-Ln**. The byproducts are hexane-soluble $Cp^*_2LnPh(THF)$, **2-Ln** (Figure S1; Tables S3 and S4) and poorly soluble $KBPh_4$, which precipitates along with graphite.

Diffusion of diethyl ether into THF solutions of the products at −35°C afforded crystals of **1-Tb** and **1-Dy** suitable for X-ray analysis (Figure 1; Tables S1 and S2). The formation and stabilization of an unexpected cyclo-Bi_6^{6-} unit is supported by observations made in organobismuth chemistry. Organobismuth compounds with non-bulky substituents can rearrange to give flexible Bi homocycles, with equilibria between rings of different size or polymers in solution.[38,40] These compounds are the first examples of a cyclic Bi hexamer in an organometallic complex with any metal. The closest structural moiety that contains six bismuth ions is an icosahedral intermetalloid cluster containing nickel ions.[33]

Solid-state structural characterization

Complexes **1-Tb** and **1-Dy** are isostructural and crystallize in the monoclinic space group $P2_1/n$. As is shown in Figure 1, the two Ln^{III} centers are bridged by a Bi_6^{6-} Zintl unit with the chair confirmation observed for cyclohexane, with the metal centers forming a distorted cube. Each Ln^{III} center is coordinated by one Cp* ligand, with

a Ln–Cp* ring centroid distance of 2.338(1) and 2.365(1) Å for **1-Tb** and **1-Dy**, respectively, and has three close Bi neighbors (see Figure 1). The edges of the Ln_2Bi_6 cube exhibit similar lengths. The Bi–Bi distances of 3.029(1)–3.042(1) Å and 3.027(1)–3.036(1) Å for **1-Tb** and **1-Dy**, respectively, are significantly longer than multiple Bi–Bi bonds (2.82–2.87 Å), and are comparable with Bi–Bi single bonds (>2.99 Å).[41] This observation suggests that the linkages between the Bi centers in **1-Ln** may be described as single bonds, as would be expected stereochemically given the chair conformation of the Bi_6^{6-} unit.

The Ln–Bi distances are 3.055(1)–3.070(1) and 3.042(1)–3.060(1) Å for **1-Tb** and **1-Dy**, respectively, approximately 0.2 Å shorter than the 3.287 Å Sm–Bi bonds.[28] This difference may be explained by three factors. First, the shorter Ln–Bi bonds are a direct result of the smaller radii of the Tb^{III} and Dy^{III} ions as compared with Sm^{III} owing to the lanthanide contraction.[42] Second, the Bi unit in the Sm complex has a higher bond order, and the greater electron density localized in multiply bonded Bi units leads to relatively weaker donating ability to Ln centers, in contrast with the situation in **1-Ln**. Third, the Tb^{III} and Dy^{III} ions in **1-Ln** are hexacoordinate, allowing the lanthanides closer to the bismuth core than may be possible in the dinuclear Sm complex, which features an eight-coordinate Sm^{III} ion. The Ln–Bi distances are shorter than the sum of the covalent radii of Ln and Bi, 3.42 and 3.40 Å for Tb and Dy, respectively.[42] This shortness indicates significant bonding interactions between Ln and Bi ions and possibly signals strong covalency (although unlikely involving the 4*f*-orbitals). Indeed, a few organometallic and intermetalloid endohedral lanthanide compounds are inferred to involve increased covalency of the lanthanide centers when supported with donor ligands that consist of heavy main group elements.[20,32] For example, calculations on $[Ln@Sn_4Bi_9]^{4-}$ (Ln = La, Ce) indicated a delocalization of the free electron pair on one Bi site to the empty d_z^2-orbital of the Ln center.[32]

The Ln_2Bi_6 core is compressed along the body diagonal between the two Ln centers, with distances of 4.043(1) and 4.034(1) Å between Tb and Dy centers, respectively, compared with an average distance of 5.632(1) and 5.617(1) Å between the corresponding diagonally opposite Bi centers. The Bi–Ln–Bi angles range from 101.02(2)°–102.19(2)° and 101.06(2)°–102.45(2)° for **1-Tb** and **1-Dy**, respectively, larger than the 90° angle for an ideal cube. The Ln_2Bi_6 core represents the first example of a heterometallocubane containing bismuth and *f*-block metal ions. The chair conformation adopted by the Bi_6 moiety, with a 6-fold negative charge, is unprecedented. The only other compound known to contain a cyclic Bi_6 unit occurs in $[Ni_x@Bi_6Ni_6(CO)_8]^{4-}$ in which the Bi_6 unit carries a 4− charge.[33] In the complexes **1-Ln**, the large negative charge of the Bi_6^{6-} anion is stabilized by the coordination of two dicationic $[Cp^*Ln^{III}]^{2+}$ moieties. The closest structural analog to **1-Ln** of which we are aware is a bimetallic niobium complex $[(\eta^6\text{-}C_6H_5Me)_2Nb_2Sn_6]^{2-}$, featuring η^6-coordinated toluene and a cyclohexane-like Zintl ion Sn_6^{12-}, which is stabilized by two Nb^V centers.[43] The crystal structures of **1-Tb** and **1-Dy** feature dianionic $[Cp^*_2Ln_2Bi_6]^{2-}$ units, each of which is surrounded by four K^+ counterions coordinated by four THF molecules in equatorial positions (Figure S2). The K^+ ions reside 3.851(4)–3.931(4) and 3.851(5)–3.955(5) Å from the Bi sites of **1-Tb** and **1-Dy**, respectively, well outside of bonding distance. The intermolecular Ln···Ln distances are also large, with more than 10 Å between adjacent $[Cp^*_2Ln_2Bi_6]^{2-}$ fragments (Figure S2).

Computational studies

To probe the electronic structure at the Ln ions in **1-Tb** and **1-Dy**, we have performed complete active space self-consistent field spin-orbit (CASSCF-SO) calculations on $[Cp^*_2Ln_2Bi_6]^{2-}$ fragments. All calculations were performed using OpenMolcas

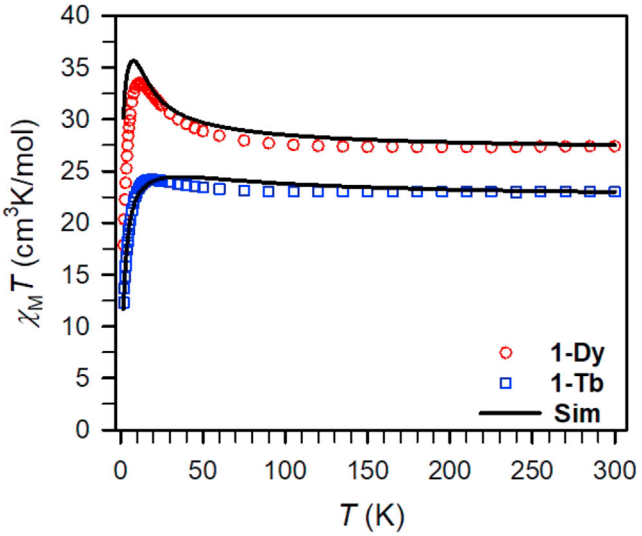

Figure 2. Dc magnetic susceptibility data for 1-Dy (red circles) and 1-Tb (blue squares) collected under a 1 kOe applied dc field

The black solid lines represent simulations using Hamiltonian 1 in the main text, with parameters $g_J = 1.30$ and $J_x = J_y = J_z = 1.0$ cm^{-1} for **1-Dy**, and $g_J = 1.46$, $J_x = J_y = -0.07$ cm^{-1} and $J_z = 2.77$ cm^{-1} for **1-Tb**.

21.06[44] with unoptimized structures from single-crystal X-ray diffraction (XRD), where only one Ln^{III} ion was considered using an 8 in 7 or 9 in 7 active space (for **1-Tb** and **1-Dy**, respectively), whereas the other ion was computationally replaced with diamagnetic Lu^{III} (see supplemental information for details). We find that, in both compounds, the crystal field experienced by the Ln^{III} ions is very small, with a total splitting of 64 and 128 cm^{-1} for **1-Tb** and **1-Dy**, respectively (Tables S5 and S6); this is in stark contrast to the large crystal field splitting known for bis-Cp^R Ln^{III} complexes of Tb^{III} and Dy^{III}.[5,45] Thus, the Bi_6^{6-} Zintl ion is clearly providing a significant effectively equatorial crystal field potential that counteracts the large axial crystal field potential generated by the Cp* ligand. Indeed, the easy magnetic axis of the ground (pseudo-)doublets are perpendicular to the Ln–Cp centroids in both cases (Figure S3), showing that the magnetic anisotropy at the metal is not dominated by the Cp* ligand and that the Bi_6^{6-} Zintl ion has a significant influence. Given the small crystal field splitting, it is unsurprising that there is considerable mixing of all the m_J functions and substantial rhombic character to the states (Tables S5 and S6). The equatorial nature of the crystal field potential generated by the Bi_6^{6-} Zintl ion appears to be a simple case of geometry: compared with the charge-dense anionic Cp* ligand, which generates a strong axial potential, the Ln^{III} ion sits just above a set of three formally Bi^{1-} anions with a local piano-stool geometry (Figure 1, bottom). The Cp*$_{centroid}$-Dy–Bi angles for these three nearest atoms are between 116° and 117°, which fall on the equatorial side of the "magic angle" of 125° for the axially symmetric crystal field parameter B_2^0 in point-charge crystal field theory,[46] where the influence of the ligand switches from axial to equatorial; hence, even from simple models, the Bi_6^{6-} Zintl ion would be expected to compete with the Cp* ligand.

Magnetic susceptibility measurements

Direct current (dc) magnetic susceptibility measurements were carried out on polycrystalline samples of **1-Ln** in an applied dc magnetic field of 1 kOe in 2 to 300 K (Figure 2). The $\chi_M T$ values at 300 K for **1-Dy** and **1-Tb** are 27.39 and 23.02 cm^3 K mol^{-1},

which are slightly lower than those expected for two non-interacting Ln^{III} ions (28.34 and 23.64 cm^3 K mol^{-1} for Dy^{III} and Tb^{III}, respectively).[47] As the temperature was lowered, an increase in $\chi_M T$ is observed with maxima of 33.49 cm^3 K mol^{-1} at 12 K and 24.18 cm^3 K mol^{-1} at 19 K for **1-Dy** and **1-Tb**, respectively. This significant increase in $\chi_M T$ is surprising, given the lack of radical-bridging ligands, and indicates that our strategy to engender strong superexchange coupling between the two Ln centers through the Bi_6^{6-} Zintl ion has been successful. Ferromagnetic interactions were confirmed by field-dependent magnetization measurements below 10 K (Figure S4), which demonstrate a rapid increase at low magnetic fields, whereas at the highest magnetic field of 7 T the magnetization remains unsaturated suggesting the presence of significant magnetic anisotropy and/or low-lying excited states.[48]

The theory of magnetic coupling between ions with unquenched orbital angular momentum is non-trivial,[49] but a simplified model proposed by Lines,[50] where only the spin-dependent part of the exchange is included (Equation 1), can be used to provide an order-of-magnitude estimate for the exchange coupling. Although this approach is a vast oversimplification,[51] and indeed, spectroscopic techniques, such as cryogenic multi-frequency electron paramagnetic resonance, are needed to obtain the details of the anisotropic exchange tensor,[2,52,53] it is useful for comparing the strength of magnetic coupling between different systems in a simple manner.

$$\mathcal{H} = \sum_{i=1,2}\sum_{k=2,4,6}\sum_{q=-k}^{k} B_k^q \hat{O}_{k_i}^q + \mu_B g_J(\hat{J}_1 + \hat{J}_2)\cdot\vec{B} - 2\left(J_x \hat{S}_{1,x}\hat{S}_{2,x} + J_y \hat{S}_{1,y}\hat{S}_{2,y} + J_z \hat{S}_{1,z}\hat{S}_{2,z}\right) \quad \text{(Equation 1)}$$

Here, the first term is the crystal field potential for each Ln^{III} ion (simplified due to the inversion symmetry), the second term is the effect of the magnetic field (Zeeman term), and the third term is the spin-spin exchange between the true-spins of the Ln^{III} ions; the z axis is defined along the Ln^{III}-$Cp^*_{centroid}$ direction, which coincides with the crystal field quantization axis. Simulations of the magnetic susceptibility data using PHI,[54] with B_k^q values fixed from CASSCF-SO calculations, suggest that $g_J \approx 1.30$ and $J_x = J_y = J_z \approx 1.0$ cm^{-1} for **1-Dy**, whereas $g_J \approx 1.46$, $J_x = J_y \approx -0.07$ cm^{-1} and $J_z \approx 2.77$ cm^{-1} for **1-Tb** (Figure 2). The fitted values of g_J are lower than expected for the free-ion Landé *g*-values of 4/3 and 3/2 for Dy^{III} and Tb^{III}, respectively, which is likely a consequence of a small uncertainty in sample mass (*ca.* 3%–5%) rather than a real effect. Interestingly, although an isotropic exchange coupling provides a sufficient simulation of the data for **1-Dy**, the exchange must be significantly anisotropic to approach the shape observed for **1-Tb**; an anisotropic model is also possible for **1-Dy** with parameters $J_x = J_y \approx -0.6$ cm^{-1} and $J_z \approx 1.5$ cm^{-1}, which shows very similar agreement to the data (Figure S5) as the isotropic model (Figure 2). Given the highly mixed crystal field states of the Ln^{III} ions obtained from CASSCF-SO, it is not fruitful to describe the coupled states in terms of m_J composition. However, both the isotropic and anisotropic models of **1-Dy** lead to an easy-axis ground pseudo-doublet with effective *g*-value of *ca.* 32 along the z axis of the compound, explaining the increase in $\chi_M T$ at low temperatures. The spectrum of excited states consists of many low-lying singlets, with the lowest group of four between 12–18 cm^{-1} (Figure S6). The case of **1-Tb** is more complicated; here, there is a manifold of six low-lying states within 5 cm^{-1} that lead to rhombic anisotropy where the x axis is the easy axis, the z axis is the intermediate axis and the y axis is the hard axis (Figure S7), explaining the less-significant rise in $\chi_M T$ compared with **1-Dy**. This likely occurs for

1-Tb due to the smaller crystal field splitting than in **1-Dy**. Due to the presence of low-lying excited states in the crystal field spectra of both compounds, it is inappropriate to use a dipolar model of magnetic interaction; therefore, we do not separate these simulated *J* values into superexchange and dipolar contributions. However, given the reasonably large distance between the Ln^{III} ions and the lack of strong uniaxial magnetic anisotropy in the ground crystal field states in either case, we suspect that the dipolar contribution is small and that the overall interaction is dominated by superexchange; this is supported by the observation of an easy-axis-type ground state for **1-Dy** along the z axis, despite the local main anisotropy directions for the ground Kramers doublet lying in the xy-plane.

The magnetic relaxation dynamics of **1-Dy** and **1-Tb** were probed by variable-frequency and variable-temperature alternating current (ac) magnetic susceptibility measurements under a 3 Oe oscillating ac field at zero dc field. The collected ac data for both compounds show frequency- and temperature-dependent out-of-phase susceptibility (χ_M'') signals (Figures 3 and S8), implying slow magnetic relaxation, typical for SMM behavior. Under ac frequencies ranging from 0.1 to 941 Hz at temperatures between 2 and 16 K for **1-Dy**, the χ_M'' peak maxima changes frequency over the entire investigated temperature range. The ac magnetic susceptibility data were used to generate Cole-Cole plots at each temperature (Figure S9), which were fitted to a generalized Debye model to extract the magnetic relaxation times (τ) distribution parameters ($0.02 < \alpha < 0.13$, revealing a narrow distribution of relaxation processes[1]). The relaxation times were employed to construct Arrhenius plots ($\ln\tau$ versus $1/T$, Figure 4). A satisfactory fit of the data requires two Orbach processes, affording barriers to spin relaxation of $U_{eff,1} = 16.9(1)\ cm^{-1}$ with $\tau_{0,1} = 7.2(1) \times 10^{-5}$ s and $U_{eff,2} = 43(2)\ cm^{-1}$ with $\tau_{0,2} = 9(3) \times 10^{-6}$ s. The smaller spin-reversal barrier, which dictates relaxation dynamics in the < 20 K regime, almost certainly arises from the exchange-coupled manifold of low-lying states and is in good agreement with breaks among the low-lying set of exchange states in **1-Dy** (for both exchange models, Figure S6). The larger barrier is harder to define owing to the small crystal field splitting and non-negligible exchange interactions. However, as this relaxation process dominates in the higher temperature regime > 20 K and its energy is quite close to the second excited state in the crystal field manifold of the individual ions (which is the first one having its main magnetic axis perpendicular to that of the ground state, Table S5), we suspect that this relaxation pathway arises from the individual Dy^{III} ions behaving as if uncoupled.

For **1-Tb**, from 2 to 2.4 K, under ac frequencies ranging from 0.1 to 941 Hz, the χ_M'' peak is temperature independent, indicating the occurrence of a QTM relaxation process in this temperature regime. Above 2.4 K and until 10 K, the χ_M'' becomes temperature dependent, hinting at an approach to an Orbach relaxation mechanism (Figure S8). Temperature-independent regimes can be effectively eliminated by application of dc fields, and ac susceptibility measurements for **1-Tb** with dc fields of 500 to 2,000 Oe resulted in differing shapes and positions of χ_M'' signals (Figure S10). With increasing dc field, the χ_M'' peak shifted to lower frequencies, which for fields higher than 1,000 Oe the χ_M'' peak maximum decreases in intensity, thus giving an optimal dc field of 1,000 Oe. Variable-temperature ac magnetic susceptibility measurements at 1,000 Oe show stronger temperature- and frequency-dependent χ_M'' peaks, especially at lower temperatures, showing effective suppression of QTM relaxation pathways (Figure S11). Fitting the Cole-Cole plots (Figure S12) to a generalized Debye model allows us to extract the relaxation times but highlights that the distribution parameters are very large at low temperatures ($0.2 < \alpha < 0.6$ for $T < 4$ K) for both 0 and 1,000 Oe data, whereas the distribution is much smaller ($\alpha < 0.17$) at higher temperatures. Here, a satisfactory fit to the

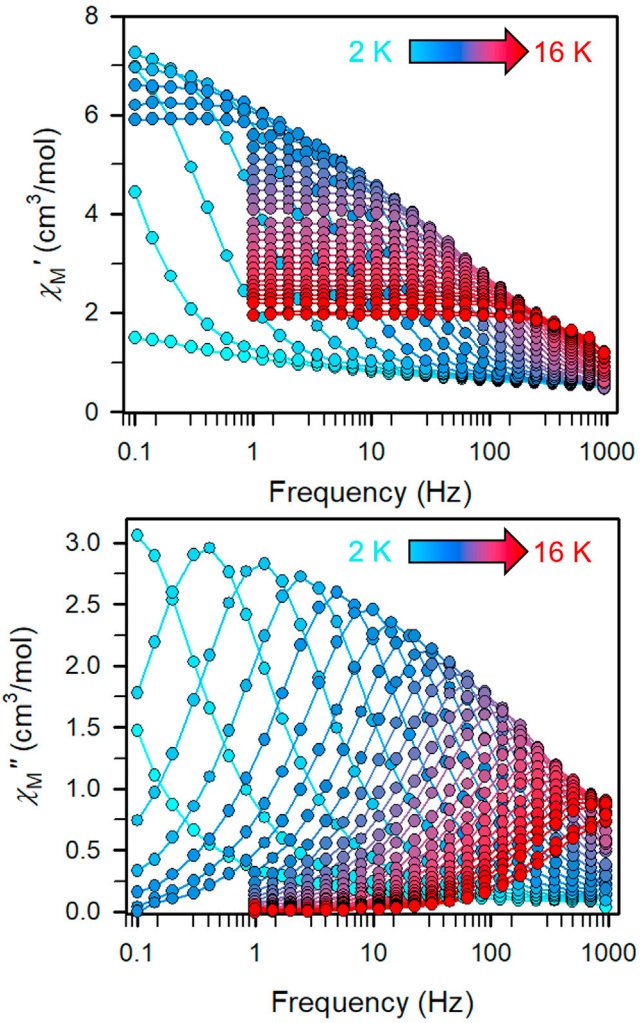

Figure 3. Variable-temperature, variable-frequency in-phase (χ_M') (top) and out-of-phase (χ_M'') (bottom) ac magnetic susceptibility data collected for 1-Dy under a zero applied dc field from 2 to 16 K

A non-zero χ_M'' out-of-phase signal indicates the presence of an energy barrier to spin reversal.

temperature-dependent relaxation times derived from zero Oe dc data required consideration of the sum of a quantum tunneling term and Orbach processes to give an effective relaxation barrier of $U_{eff} = 18.0(8)$ cm^{-1} with $\tau_0 = 1.2(5) \times 10^{-5}$ s, and a quantum tunneling relaxation time of $\tau = 0.13$ s (Figure 4); similar Orbach parameters of $U_{eff} = 19.4(1)$ cm^{-1} and $\tau_0 = 1.0(1) \times 10^{-5}$ s were obtained from the 1,000 Oe dc field data (no tunneling term required).

The performance of SMMs in high-density storage applications requires magnetization retention in the absence of dc fields. Thus, variable-field magnetization measurements were performed on polycrystalline samples of **1-Tb** and **1-Dy** at an average sweep rate of 100 Oe/s. Below 3 K, **1-Tb** exhibits waist-restricted magnetic hysteresis loops (Figure S13), consistent with the relaxation times obtained under zero dc field from ac magnetic susceptibility measurements. These loops are consistent with the presence of QTM relaxation processes. By contrast, open magnetic hysteresis loops were observed up to 4.5 K for **1-Dy** (Figure 5), with a maximum H_c of 0.271 T (Figures S14 and S15), which is remarkable due to the moderate value

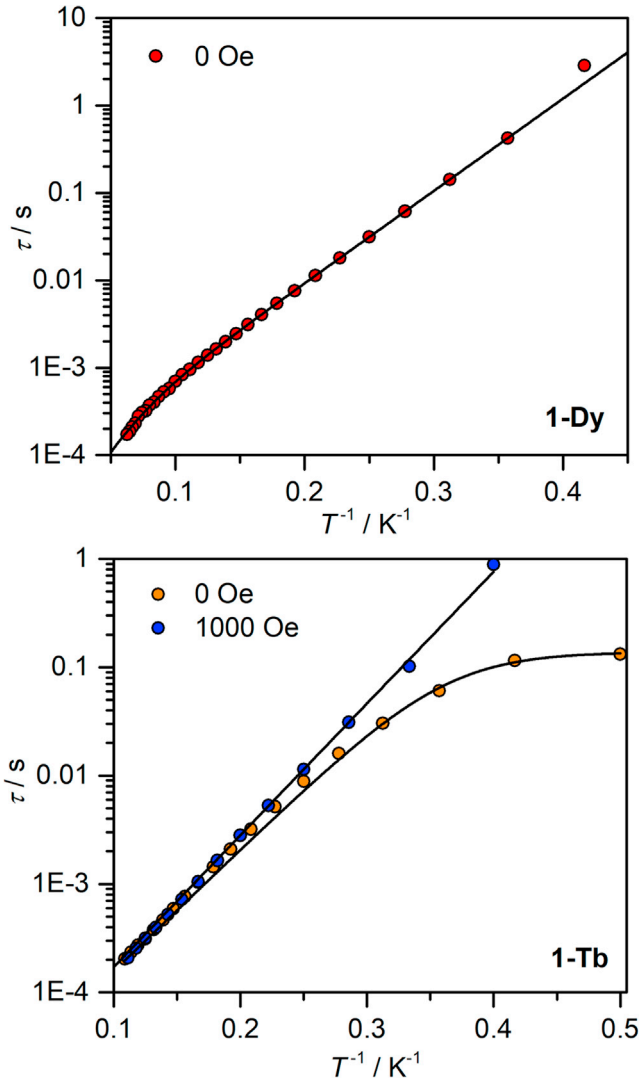

Figure 4. Plots of magnetic relaxation time (τ, log scale) versus temperature (T, inverse scale) for polycrystalline samples of 1-Dy (top) and 1-Tb (bottom)

For **1-Dy**, the black solid line represents the best fit to a sum of two Orbach processes, $\tau^{-1} = \tau_{0,1}^{-1}\exp(-U_{eff,1}/T) + \tau_{0,2}^{-1}\exp(-U_{eff,2}/T)$; for **1-Tb**, the black solid lines represent the best fit of the Oe data (orange circles) to a sum of QTM and Orbach processes, $\tau^{-1} = \tau_{QTM}^{-1} + \tau_0^{-1}\exp(-U_{eff}/T)$, and of the 1,000 Oe data (blue circles) to only one Orbach process, $\tau^{-1} = \tau_0^{-1}\exp(-U_{eff}/T)$, respectively. Standard deviations of the relaxation times were determined from a nonlinear least-squares analysis employing the program SolverAid (Version 7) by R. de Levie (Microsoft Excel Macro, 2007).

for the effective spin relaxation barrier U_{eff}. Notably, there are no prominent steplike features present at H = 0 Oe, where such steps in hysteresis loops are generally occurring for lanthanide-based SMMs. The absence of steps indicates an effective suppression of QTM relaxation processes[2] and is attributed to presence of superexchange interactions.

Our results show that significant superexchange with contracted 4*f*-orbitals, SMM behavior and magnetic blocking can be attained in the first series of bimetallic lanthanide molecules with an unprecedented bridging bismuth cluster. The preparation of these unique compounds proceeded via an organometallic approach in

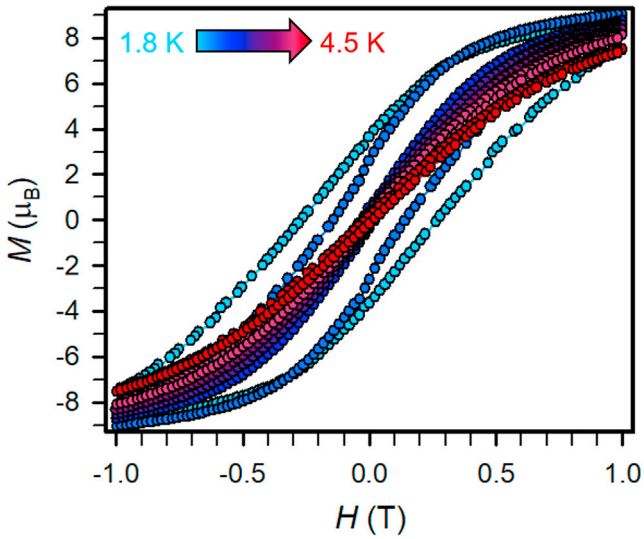

Figure 5. Variable-field magnetization data for 1-Dy collected from 1.8 to 4.5 K at an average sweep rate of 100 Oe/s

See also Figures S14 and S15.

solution. The extraordinary core unit represents a distorted [Ln_2Bi_6] cuboid. The Bi_6^{6-} Zintl bridge fosters ferromagnetic interactions between the two Ln^{III} centers through a superexchange mechanism, leading to molecular exchange-based magnetic blocking and open magnetic hysteresis at low temperatures for the Dy congener. These results highlight the potential of heavy main group elements in mediating magnetic exchange interactions between Ln^{III} centers and open up new ways to construct exchange-coupled SMMs that show magnetic blocking.

EXPERIMENTAL PROCEDURES

Resource availability

Lead contact

Further information and requests for resources should be directed to and will be fulfilled by the lead contact, Selvan Demir (sdemir@chemistry.msu.edu).

Materials availability

This study did not generate new reagents.

Data and code availability

The accession numbers for the crystallographic data reported in this paper are CCDC: 2074919, 2074923, 2074924, 2074925. Copies of these data can be obtained free of charge from the Cambridge Crystallographic Data Centre via www.ccdc.cam.ac.uk/data_request/cif. Correspondence and requests for materials should be addressed to Selvan Demir.

All manipulations were carried out under an inert atmosphere of dry nitrogen using Schlenk or glove box techniques. Compounds were characterized by single-crystal X-ray diffraction, elemental analysis, IR spectroscopy, and variable-temperature SQUID magnetometry.

Preparation of $[K(THF)_4]_2[Cp^*_2Dy_2Bi_6]$, 1-Dy

In an argon-filled glovebox, 23.5 mg (0.053 mmol) $BiPh_3$ and 134.8 mg (0.179 mmol) $Cp^*_2Dy(BPh_4)$[35] were weighed into a 20 mL scintillation vial and dissolved in 4 mL

THF. The solution was heated to 45°C and stirred for 5 min to dissolve all solid materials. 29.4 mg (0.217 mmol) KC_8 were added and stirred for 15 min. After filtration, a clear dark red solution was obtained. The solvent was removed under vacuum to afford a dark solid, which was washed twice with 5 mL of hexane and once with 3 mL of toluene to remove the byproduct $Cp^*_2DyPh(THF)$. The residual solid was dissolved in 5 mL of THF and filtered to obtain a brown solution, which was subsequently evaporated to dryness. The remaining brown solids (~15 mg) were dissolved in 1 mL of THF, and **1-Dy** (3.5 mg) was crystallized from the THF solution through diethyl ether diffusion at −35°C in 20% yield based on $BiPh_3$. The reactions were repeated multiple times and the product collected and confirmed through elemental analysis before conducting magnetic measurements. The black crystals were suitable for X-ray analysis. Anal. Calc. for $Dy_2Bi_6C_{20}H_{30}K_2{\cdot}1THF$: C, 14.47; H, 1.92; N, 0. Found: C, 14.10; H, 2.07; N, 0.08. IR (ATR, cm^{-1}): 2,839 (br), 1,487 (w), 1,427 (m), 1,414 (m), 1,367 (s), 1,284 (w), 1,147 (s), 1,086 (s), 1,045 (s), 1,017 (s), 930 (s), 954 (w), 842 (s), 800 (s), 744 (w), 714 (w).

Preparation of $[K(THF)_4]_2[Cp^*_2Tb_2Bi_6]$, 1-Tb

Following the synthetic procedure for **1-Dy**, **1-Tb** (2.0 mg) was crystallized from THF solution through diffusion with diethyl ether at −35°C in 11% yield based on $BiPh_3$. Used masses: $BiPh_3$ (23.5 mg, 0.053 mmol), $Cp^*_2Tb(BPh_4)$ (134.2 mg, 0.179 mmol), and KC_8 (29.4 mg, 0.217 mmol). The black crystals were suitable for X-ray analysis. Anal. Calc. for $Tb_2Bi_6C_{20}H_{30}K_2{\cdot}4THF$: C, 19.58; H, 2.83; N, 0. Found: C, 19.93; H, 2.61; N, 0.20.

SUPPLEMENTAL INFORMATION

Supplemental information can be found online at https://doi.org/10.1016/j.chempr.2021.11.007.

ACKNOWLEDGMENTS

S.D. thanks Michigan State University and the Department of Chemistry at MSU for generous start-up funding. Funding for the single-crystal X-ray diffractometer was provided by the MRI program by the National Science Foundation under grant no. 1919565. N.F.C. thanks the Royal Society for a University Research Fellowship (URF191320) and the University of Manchester for support. We thank Dr. Richard Staples for helpful discussions and Elizabeth Pugliese for experimental assistance.

AUTHOR CONTRIBUTIONS

P.Z. and F.B. prepared and characterized the compounds. P.Z. and S.D. carried out and interpreted the SQUID magnetometry. P.Z. and F.B. collected, solved, and refined the X-ray diffraction data. N.F.C. performed CASSCF-SO calculations and spin Hamiltonian modeling. S.D. assisted with data analysis, formulated and directed the research, and wrote the manuscript with input from all the authors.

DECLARATION OF INTERESTS

The authors declare no competing interests.

Received: April 25, 2021
Revised: October 4, 2021
Accepted: November 9, 2021
Published: December 2, 2021

REFERENCES

1. Gatteschi, D., Sessoli, R., and Vallain, J. (2006). Molecular Nanomagnets (Oxford University Press).

2. Moreno Pineda, E., Chilton, N.F., Marx, R., Dörfel, M., Sells, D.O., Neugebauer, P., Jiang, S.-D., Collison, D., van Slageren, J., McInnes, E.J.L., and Winpenny, R.E.P. (2014). Direct measurement of dysprosium(III)'dysprosium(III) interactions in a single-molecule magnet. Nat. Commun. *5*, 5243.

3. Woodruff, D.N., Winpenny, R.E.P., and Layfield, R.A. (2013). Lanthanide single-molecule magnets. Chem. Rev. *113*, 5110–5148.

4. Rinehart, J.D., and Long, J.R. (2011). Exploiting single-ion anisotropy in the design of *f*-element single-molecule magnets. Chem. Sci. *2*, 2078–2085.

5. Guo, F.-S., Day, B.M., Chen, Y.-C., Tong, M.-L., Mansikkamäki, A., and Layfield, R.A. (2018). Magnetic hysteresis up to 80 kelvin in a dysprosium metallocene single-molecule magnet. Science *362*, 1400–1403.

6. Rinehart, J.D., Fang, M., Evans, W.J., and Long, J.R. (2011). Strong exchange and magnetic blocking in N_2^{3-} radical-bridged lanthanide complexes. Nat. Chem. *3*, 538–542.

7. Mondal, K.C., Sundt, A., Lan, Y., Kostakis, G.E., Waldmann, O., Ungur, L., et al. (2012). Coexistence of distinct single-ion and exchange-based mechanisms for blocking of magnetization in a $Co(II)_2Dy(III)_2$ single-molecule magnet. Angew. Chem. Int. Ed. Engl. *51*, 7550–7554.

8. Langley, S.K., Wielechowski, D.P., Vieru, V., Chilton, N.F., Moubaraki, B., Abrahams, B.F., et al. (2013). A $\{Cr(III)_2Dy(III)_2\}$ single-molecule magnet: enhancing the blocking temperature through 3*d* magnetic exchange. Angew. Chem. Int. Ed. Engl. *52*, 12014–12019.

9. Wang, J., Li, Q.-W., Wu, S.-G., Chen, Y.-C., Wan, R.-C., Huang, G.-Z., Liu, Y., Liu, J.-L., Reta, D., Giansiracusa, M.J., et al. (2021). Opening magnetic hysteresis by axial ferromagnetic coupling: from mono-decker to double-decker metallacrown. Angew. Chem. Int. Ed. Engl. *60*, 5299–5306.

10. Demir, S., Jeon, I.-R., Long, J.R., and Harris, T.D. (2015). Radical ligand-containing single-molecule magnets. Coord. Chem. Rev. *289*, 149–176.

11. Liu, F., Spree, L., Krylov, D.S., Velkos, G., Avdoshenko, S.M., and Popov, A.A. (2019). Single-electron lanthanide-lanthanide bonds inside fullerenes toward robust redox-active molecular magnets. Acc. Chem. Res. *52*, 2981–2993.

12. Liu, F., Velkos, G., Krylov, D.S., Spree, L., Zalibera, M., Ray, R., Samoylova, N.A., Chen, C.-H., Rosenkranz, M., Schiemenz, S., et al. (2019). Air-stable redox-active nanomagnets with lanthanide spins radical-bridged by a metal–metal bond. Nat. Commun. *10*, 571.

13. Demir, S., Gonzalez, M.I., Darago, L.E., Evans, W.J., and Long, J.R. (2017). Giant coercivity and high magnetic blocking temperatures for N23− radical-bridged dilanthanide complexes upon ligand dissociation. Nat. Commun. *8*, 2144.

14. Gould, C.A., Mu, E., Vieru, V., Darago, L.E., Chakarawet, K., Gonzalez, M.I., Demir, S., and Long, J.R. (2020). Substituent effects on exchange coupling and magnetic relaxation in 2,2′-bipyrimidine radical-bridged dilanthanide complexes. J. Am. Chem. Soc. *142*, 21197–21209.

15. Guo, F.S., Bar, A.K., and Layfield, R.A. (2019). Main group chemistry at the interface with molecular magnetism. Chem. Rev. *119*, 8479–8505.

16. Tuna, F., Smith, C.A., Bodensteiner, M., Ungur, L., Chibotaru, L.F., McInnes, E.J.L., Winpenny, R.E.P., Collison, D., and Layfield, R.A. (2012). A high anisotropy barrier in a sulfur-bridged organodysprosium single-molecule magnet. Angew. Chem. Int. Ed. Engl. *51*, 6976–6980.

17. Pugh, T., Tuna, F., Ungur, L., Collison, D., McInnes, E.J.L., Chibotaru, L.F., and Layfield, R.A. (2015). Influencing the properties of dysprosium single-molecule magnets with phosphorus donor ligands. Nat. Commun. *6*, 7492.

18. Pugh, T., Vieru, V., Chibotaru, L.F., and Layfield, R.A. (2016). Magneto-structural correlations in arsenic- and selenium-ligated dysprosium single-molecule magnets. Chem. Sci. *7*, 2128–2137.

19. Pugh, T., Chilton, N.F., and Layfield, R.A. (2017). Antimony-ligated dysprosium single-molecule magnets as catalysts for stibine dehydrocoupling. Chem. Sci. *8*, 2073–2080.

20. Chen, S.-M., Xiong, J., Zhang, Y.-Q., Ma, F., Sun, H.-L., Wang, B.-W., et al. (2019). Dysprosium complexes bearing unsupported Dy^{III}–Ge^{II}/Sn^{II} metal-metal bonds as single-ion magnets. Chem. Commun. (Camb) *55*, 8250–8253.

21. Chen, C.-H., Krylov, D.S., Avdoshenko, S.M., Liu, F., Spree, L., Yadav, R., et al. (2017). Selective arc-discharge synthesis of Dy_2S-clusterfullerenes and their isomer-dependent single molecule magnetism. Chem. Sci. *8*, 6451–6465.

22. Sessoli, R., Gatteschi, D., Caneschi, A., and Novak, M.A. (1993). Magnetic bistability in a metal-ion cluster. Nature *365*, 141–143.

23. de Marcillac, P., Coron, N., Dambier, G., Leblanc, J., and Moalic, J.-P. (2003). Experimental detection of α-particles from the radioactive decay of natural bismuth. Nature *422*, 876–878.

24. Lichtenberg, C. (2016). Well-defined, mononuclear Bi^{I} and Bi^{II} compounds: towards transition-metal-like behavior. Angew. Chem. Int. Ed. Engl. *55*, 484–486.

25. Pearson, T.J., Fataftah, M.S., and Freedman, D.E. (2016). Enhancement of magnetic anisotropy in a Mn–Bi heterobimetallic complex. Chem. Commun. (Camb) *52*, 11394–11397.

26. Rookes, T.M., Wildman, E.P., Balázs, G., Gardner, B.M., Wooles, A.J., Gregson, M., Tuna, F., Scheer, M., and Liddle, S.T. (2018). Actinide–pnictide (An−Pn) bonds spanning non-metal, metalloid, and metal combinations (An=U, Th; Pn=P, As, Sb, Bi). Angew. Chem. Int. Ed. Engl. *57*, 1332–1336.

27. Eulenstein, A.R., Franzke, Y.J., Lichtenberger, N., Wilson, R.J., Deubner, H.L., Kraus, F., et al. (2021). Substantial π-aromaticity in the anionic heavy-metal cluster $[Th@Bi_{12}]^{4-}$. Nat. Chem. *13*, 149–155.

28. Evans, W.J., Gonzales, S.L., and Ziller, J.W. (1991). Organosamarium-mediated synthesis of bismuth-bismuth bonds: X-ray crystal structure of the first dibismuth complex containing a planar $M_2(\mu\text{-}\eta^2\text{:}\eta^2\text{-}Bi_2)$ unit. J. Am. Chem. Soc. *113*, 9880–9882.

29. Lips, F., Clérac, R., and Dehnen, S. (2011). $[Eu@Sn_6Bi_8]^{4-}$: a mini-fullerane-type zintl anion containing a lanthanide ion. Angew. Chem. Int. Ed. *50*, 960–964.

30. Weinert, B., Müller, F., Harms, K., Clérac, R., and Dehnen, S. (2014). Origin and location of electrons and protons during the formation of intermetalloid clusters $[Sm@Ga_{3-x}H_{3-2x}Bi_{10+x}]^{3-}$ (x=0, 1). Angew. Chem. Int. Ed. Engl. *53*, 11979–11983.

31. Weinert, B., Weigend, F., and Dehnen, S. (2012). Subtle impact of atomic ratio, charge and Lewis basicity on structure selection and stability: the zintl anion $[(La@In_2Bi_{11})(\mu\text{-}Bi)_2(La@In_2Bi_{11})]^{6-}$. Chemistry *18*, 13589–13595.

32. Lips, F., Hołyńska, M., Clérac, R., Linne, U., Schellenberg, I., Pöttgen, R., et al. (2012). Doped semimetal clusters: ternary, intermetalloid anions $[Ln@Sn_7Bi_7]^{4-}$ and $[Ln@Sn_4Bi_9]^{4-}$ (Ln = La, Ce) with adjustable magnetic properties. J. Am. Chem. Soc. *134*, 1181–1191.

33. Goicoechea, J.M., Hull, M.W., and Sevov, S.C. (2007). Heteroatomic deltahedral clusters: synthesis and structures of *closo*-$[Bi_3Ni_4(CO)_6]^{3-}$, *closo*-$[Bi_4Ni_4(CO)_6]^{2-}$, the open cluster $[Bi_3Ni_6(CO)_9]^{3-}$, and the intermetalloid *closo*-$[Ni_x@\{Bi_6Ni_6(CO)_8\}]^{4-}$. J. Am. Chem. Soc. *129*, 7885–7893.

34. Min, X., Popov, I.A., Pan, F.-X., Li, L.-J., Matito, E., Sun, Z.-M., et al. (2016). All-metal antiaromaticity in Sb_4-type lanthanocene anions. Angew. Chem. Int. Ed. Engl. *55*, 5531–5535.

35. Wilson, R.J., Lichtenberger, N., Weinert, B., and Dehnen, S. (2019). Intermetalloid and heterometallic clusters combining *p*-block (semi)metals with *d*- or *f*-block metals. Chem. Rev. *119*, 8506–8554.

36. Schenk, C., and Schnepf, A. (2007). $[AuGe_{18}\{Si(SiMe_3)_3\}_6]^-$: a soluble Au–Ge cluster on the way to a molecular cable? Angew. Chem. Int. Ed. Engl. *46*, 5314–5316.

37. Woen, D.H., and Evans, W.J. (2016). Chapter 293. Expanding the +2 oxidation state of the rare-earth metals, uranium, and thorium in molecular complexes. In Handbook on the Physics and Chemistry of Rare Earths, J.-C.G. Bünzli and V.K. Pecharsky, eds. (Elsevier), pp. 337–394.

38. Balázs, L., and Breunig, H.J. (2004). Organometallic compounds with Sb–Sb or Bi–Bi bonds. Coord. Chem. Rev. *248*, 603–621.

39. Demir, S., Zadrozny, J.M., Nippe, M., and Long, J.R. (2012). Exchange coupling and magnetic blocking in bipyrimidyl radical-bridged dilanthanide complexes. J. Am. Chem. Soc. *134*, 18546–18549.

40. Breunig, H.J., Rösler, R., and Lork, E. (1998). The first organobismuth rings: $(RBi)_3$ and $(RBi)_4$, $R=(Me_3Si)_2CH$. Angew. Chem. Int. Ed. Engl. *37*, 3175–3177.

41. Jones, J.S., Pan, B., and Gabbaï, F.P. (2015). Group 15 metal-metal bonds. Molecular Metal-Metal Bonds, 519–558. https://doi.org/10.1002/9783527673353.ch15.

42. Cordero, B., Gómez, V., Platero-Prats, A.E., Revés, M., Echeverría, J., Cremades, E., Barragán, F., and Alvarez, S. (2008). Covalent radii revisited. Dalton Trans. 2832–2838.

43. Kesanli, B., Fettinger, J., and Eichhorn, B. (2001). The $[(\eta\text{-}C_6H_5Me)NbSn_6Nb(\eta\text{-}C_6H_5Me)]^{2-}$ ion: a complex containing a metal-stabilized Sn_6^{12-} cyclohexane-like zintl ion. Angew. Chem. Int. Ed. Engl. *40*, 2300–2302.

44. Galván, I.F., Vacher, M., Alavi, A., Angeli, C., Aquilante, F., Autschbach, J., Bao, J.J., Bokarev, S.I., Bogdanov, N.A., Carlson, R.K., et al. (2019). OpenMolcas: from source code to insight. J. Chem. Theory Comput. *15*, 5925–5964.

45. Goodwin, C.A.P., Reta, D., Ortu, F., Chilton, N.F., and Mills, D.P. (2017). Synthesis and electronic structures of heavy lanthanide metallocenium cations. J. Am. Chem. Soc. *139*, 18714–18724.

46. Sorace, L., Benelli, C., and Gatteschi, D. (2011). Lanthanides in molecular magnetism: old tools in a new field. Chem. Soc. Rev. *40*, 3092–3104.

47. Benelli, C., and Gatteschi, D. (2002). Magnetism of lanthanides in molecular materials with transition-metal ions and organic radicals. Chem. Rev. *102*, 2369–2388.

48. Lin, P.H., Burchell, T.J., Clérac, R., and Murugesu, M. (2008). Dinuclear dysprosium(III) single-molecule magnets with a large anisotropic barrier. Angew. Chem. Int. Ed. Engl. *47*, 8848–8851.

49. Iwahara, N., and Chibotaru, L.F. (2015). Exchange interaction between *J* multiplets. Phys. Rev. B *91*, 174438.

50. Lines, M.E. (1971). Orbital angular momentum in the theory of paramagnetic clusters. J. Chem. Phys. *55*, 2977–2984.

51. Ortu, F., Liu, J., Burton, M., Fowler, J.M., Formanuik, A., Boulon, M.E., Chilton, N.F., and Mills, D.P. (2017). Analysis of lanthanide-radical magnetic interactions in Ce(III) 2,2′-bipyridyl complexes. Inorg. Chem. *56*, 2496–2505.

52. Giansiracusa, M.J., Moreno-Pineda, E., Hussain, R., Marx, R., Martínez Prada, M., Neugebauer, P., Al-Badran, S., Collison, D., Tuna, F., van Slageren, J., et al. (2018). Measurement of magnetic exchange in asymmetric lanthanide dimetallics: toward a transferable theoretical framework. J. Am. Chem. Soc. *140*, 2504–2513.

53. Giansiracusa, M.J., Al-Badran, S., Kostopoulos, A.K., Whitehead, G.F.S., McInnes, E.J.L., Collison, D., Winpenny, R.E.P., and Chilton, N.F. (2020). Magnetic exchange interactions in symmetric lanthanide dimetallics. Inorg. Chem. Front. *7*, 3909–3918.

54. Chilton, N.F., Anderson, R.P., Turner, L.D., Soncini, A., and Murray, K.S. (2013). PHI: a powerful new program for the analysis of anisotropic monomeric and exchange-coupled polynuclear *d*- and *f*-block complexes. J. Comput. Chem. *34*, 1164–1175.